

# Investigation of Phase Difference Statistics of Numerically Simulated High-Resolution HH- and VV-Polarized Low Grazing Angle Sea Backscatter

Jakov V. Toporkov\* and Mark A. Sletten  
Remote Sensing Division  
Naval Research Laboratory  
Washington, DC 20375-5320, USA

**Abstract**—This study uses direct numerical simulations of X-band low grazing sea backscatter to investigate phase difference statistics between the co-polarized (horizontal transmit-receive and vertical transmit-receive) channels. The range resolution is 0.4 m and the grazing angles are as low as 0.5 degrees. The simulations are limited to the two-dimensional space but have immediate relevance to commonly occurring observation geometries. Phase probability density functions are calculated using different methods (such as amplitude thresholding or multilook averaging) and are shown to differ substantially from analytical predictions based on the commonly used Gaussian-statistics assumptions. Adequate knowledge of such inter-channel phase probability distributions is important for ocean-oriented applications of radar polarimetry.

**Keywords**—scattering by rough surfaces; low grazing angles; sea clutter statistics; radar polarimetry; numerical simulations

## I. INTRODUCTION

Terrestrial applications have convincingly demonstrated that polarimetric radar measurements can be very helpful for scene classification and target detection tasks [1]. Knowledge of relative phases between polarization channels is an essential component of such analysis, and phase statistics (and more generally, joint amplitude-phase statistics) are important for algorithm development and performance predictions. To some extent, polarization diversity has been successfully employed in ocean-based studies: concurrent measurements of horizontal transmit-receive (HH) and vertical transmit-receive (VV) cross sections have been instrumental for investigations of the "sea spike" phenomenon [2], and the cross-polarized (HV or VH) radar cross-section appears to be sensitive to the surface wind speed, an important environmental parameter [3]. In these applications, however, inter-channel phases are not either measured or exploited. Some experimental fully polarimetric observations of low grazing sea backscatter have been reported [4]; still, the true potential of radar polarimetry as applied to ocean environment is yet to be understood. One issue appears to be the statistics of radar echoes from sea surface. In land

applications, a complex multi-variate Gaussian process is used to jointly describe radar backscatter at various polarizations, and expressions for phase-difference and other statistics are derived based on this assumption [1]. The sea clutter, however, is known to display non-Gaussian properties, especially in the low-grazing regime where the majority of shipborne and coastal radars operate [2]. One of the questions important for the ocean-based polarimetry is whether and how this manifestly non-Gaussian nature affects the applicability of the existing polarimetric methods and if modifications or new approaches are needed to take this into account.

We address this issue using direct numerical simulations of short-pulse scattering from ocean-like sea surfaces. The method has been used in investigating amplitude statistics of the low-grazing angle (LGA) sea backscatter [5]. In this paper, we focus on estimating the probability density function (PDF) of the relative phase between the complex HH and VV echoes. Since LGA backscatter has large proportions of very low values (that are reproduced by the numerical simulations but are likely to be masked by thermal noise in practice), the dependence of phase statistics on an amplitude threshold is of interest. A "multi-look" approach that involves averaging over a number of resolution cells, and its impact on the phase statistics are also considered. The estimated PDFs are compared to the analytical results in [1] derived based on the Gaussian assumption for the joint VV-HH backscatter probability density, and the observed differences are discussed.

## II. SIMULATION DETAILS

The problem set-up is shown in Fig.1. The wind-driven surface is represented by a realization of a Gaussian random process defined by the Elfouhaily wave spectrum [6]. Interactions between surface harmonics that are responsible, in particular, for shaping the small-scale roughness and thus impact scattering of centimeter-scale electromagnetic waves (this study uses X-band  $\lambda=3.2$  cm), are implemented through the Creamer transformation applied to a Gaussian-process realization [7]. The model does not describe wave breaking. The electromagnetic field scattered by a given surface profile at a particular frequency is found following an iterative solution of the boundary integral equation for the induced electric surface current [8]. The flat region visible in Fig.1 on the left is introduced to alleviate any possible edge effects associated

---

This work was supported by the US Naval Research Laboratory under the 6.1 Base Research Program (Work Unit 72-4280). It was also supported in part by a grant of computer time from the DoD High Performance Computing Modernization Program at the Naval Research Laboratory Distributed Center, the US Air Force Research Laboratory DoD Supercomputer Resource Center, and the US Army Space and Missile Defense Command Simulation Center.

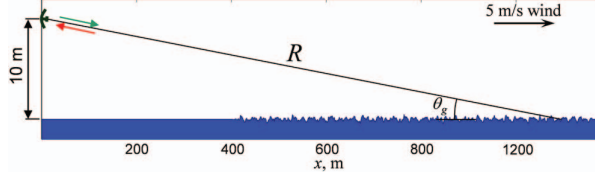


Figure 1. Problem setup and geometry

with finite surface size. The formulation automatically accounts for many phenomena (multiple scattering, shadowing) known to be problematic for analytical treatment. The surface response is calculated at 8192 frequencies, and Fourier synthesis is used to simulate backscattering of a 2.7-ns pulse with the corresponding range resolution is 0.4 m. (Power-wise, the pulse width is 1.9 ns with the range resolution being 0.29 m.) A 12.5-s temporal evolution of the surface was considered; it is represented by a sequence of 500 profiles, with scattering calculations repeated for each one. The grazing angle varies from  $1.3^\circ$  at the closer distance (where the roughness starts) down to  $0.5^\circ$  at the far end. Due to computational considerations, the simulations are limited to a two-dimensional situation and thus can produce only co-polarized (HH or VV) backscatter. Still, this setup has direct relevance to commonly occurring three-dimensional situations with a narrow-beam radar observing approaching or receding long-crested waves. Absence of thermal noise and complete knowledge of surface profiles are additional advantages of the “numerical experiment”.

### III. RESULTS

Fig. 2 gives examples of the simulated surface backscatter in response to a single radar pulse. In the magnitude plots, the effects of antenna pattern and of signal decrease with range have been compensated. Furthermore, proper normalizations are applied so that when averaged power-wise, the results should produce the normalized radar cross-section [5]. Both VV and HH magnitudes exhibit a “spiky” character with relatively sparse strong peaks and considerably lower signal levels in between. This behavior of the LGA sea clutter is well known from experimental observations, and has been reproduced in our earlier direct numerical simulations [5] that considered grazing angles down to  $5^\circ$ . While the mechanisms of such behavior are not entirely clear (note that our simulations exclude breakers), steepening waves and shadowing effects must certainly play a role.

The phase difference plot in Fig 2. is quite noise-like, with the values spanning the whole 360-degree range. However, there is apparent clustering around approximately  $30^\circ$ . This appears to be the value predicted by the first-order Small Perturbation Method (SPM1) that considers Bragg scattering by a slightly rough surface, cf. [9] for example. Namely, the SPM1 prediction is obtained as an argument of the ratio of the complex coefficients [9]

$$g_{\text{HH}} = \frac{\varepsilon - 1}{(\sin \theta_g + \sqrt{\varepsilon - \cos^2 \theta_g})^2}$$

and

$$g_{\text{VV}} = \frac{(\varepsilon - 1)\{\varepsilon + \cos^2 \theta_g (\varepsilon - 1)\}}{(\varepsilon \sin \theta_g + \sqrt{\varepsilon - \cos^2 \theta_g})^2} \quad (1)$$

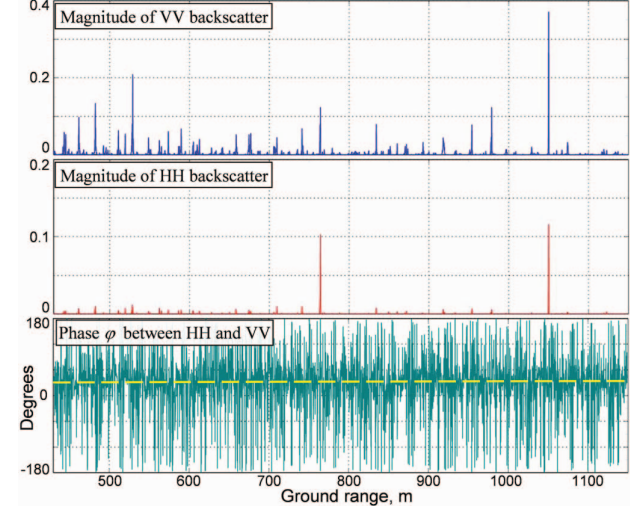


Figure 2. Magnitudes of instantaneous surface echoes and the phase difference between them. Dashed curve in the phase plot corresponds to the Bragg scattering theory (SPM1) prediction.

The relative dielectric permittivity of the sea water  $\varepsilon$  is taken to be  $55.3 - j38.9$ , and the grazing angle  $\theta_g$  is defined in Fig. 1. The resulting phase varies slightly with the grazing angle, growing from approximately  $30^\circ$  at to  $33^\circ$  as the ground range in Fig. 2 increases.

Fig. 3 displays PDFs of the VV and HH backscatter magnitudes normalized by their respective rms values [5]. To reduce the impact of clutter variability with the grazing angle, here and in what follows we will consider only the data falling within the last one-third of the ground range shown in Fig. 2; this corresponds to grazing angles between  $0.6$  and  $0.5$  degrees. Backscatter realizations from all 500 profiles representing surface evolution are used to boost the statistical ensemble. Both PDFs have long “tails”, with the HH plot decaying at a slower pace and eventually overtaking its VV counterpart. These tails are indicative of the “spiky” clutter [2]. A comparison to the Rayleigh probability density  $p_R(a) = 2a \exp(-a^2)$  that describes the magnitude of the normal process, demonstrates that the LGA backscatter statistics are clearly non-Gaussian. In fact, the K or Weibull distributions with proper shape parameters appear to be a good fit [2], [5].

The estimated PDF of phase difference between the HH and VV channels is shown in Fig. 4 (thick solid line). It is compared to the Gaussian-based analytical prediction [1]

$$p_\varphi(\varphi) = \frac{(1 - \rho^2)[(1 - \beta^2)^{1/2} + \beta(\pi - \arccos \beta)]}{2\pi(1 - \beta^2)^{3/2}} \quad (2)$$

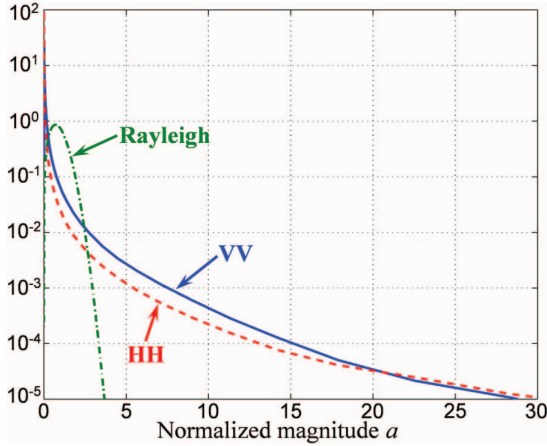


Figure 3. Probability density function of the backscatter magnitude. Rayleigh PDF is shown for reference.

with

$$\beta = \rho \cos(\varphi - \psi). \quad (3)$$

The expressions (2)-(3) contain two parameters,  $\rho$  and  $\psi$  that are magnitude and phase of the complex correlation coefficient

$$\rho_c \equiv \rho e^{j\psi} = \frac{\langle S_{HH} S_{VV}^* \rangle}{(\langle |S_{HH}|^2 \rangle \langle |S_{VV}|^2 \rangle)^{1/2}} \quad (4)$$

that can be estimated from the data. In (4),  $S_{HH}$  and  $S_{VV}$  are the components of the scattering matrix [1]; in the context of this study the normalized complex backscatter values play this role. Equation (2) assumes the argument to be in radians; if one measures phase in degrees, the expression should be multiplied by  $(\pi/180^\circ)$ . The analytical PDF (thin solid curve) is plotted in Fig. 4 for the estimated parameters  $\rho = 0.68$  and  $\psi = 17.6^\circ$ . It peaks at  $\varphi = \psi$  and tends to broaden if the coherence  $\rho$  decreases.

Since it was already noted in Fig. 3 that the LGA clutter does not follow the Gaussian statistics, it is not surprising to see differences between the estimated and the Gaussian-based analytical PDFs. The simulated backscatter probability density is narrower than the analytical prediction. Also, it peaks at a different angle that appears to be consistent with the SPM1 result, as was observed in Fig. 2. We note that the rms surface roughness of 0.16 m is much larger than the 3-cm wavelength. Because of the spikiness, the estimated phase PDF takes into account a lot of values where signal is very weak, cf. Fig. 2. Magnitude PDFs in Fig. 3 suggest that the proportion of such low-amplitude samples is high (the K and Weibull distributions used to model the LGA clutter statistics have an integrable singularity at  $a=0$ ). In practice, those weak portions of the echo signal are likely to be masked by the receiver noise; even in these “noise-free” simulations some samples may be affected by numerical artifacts. Therefore, a logical approach would be to retain phase values only when signal levels exceed certain threshold. This level is set individually for the VV and HH

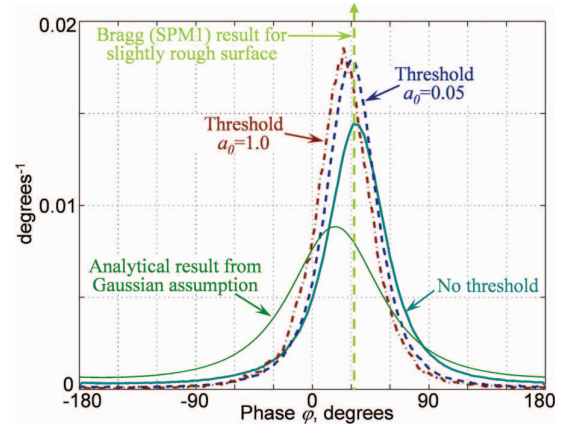


Figure 4. Probability density functions of phase difference between HH and VV backscatter evaluated from the simulated data subject to magnitude thresholding. Analytical prediction from (2) is also shown for reference.

channels as a common fraction of their respective rms magnitudes. In terms of the scaled magnitude  $a$  used in Fig. 3, the two considered threshold cases are  $a_0 = 0.05$  and  $a_0 = 1.0$ . A phase value is used in the PDF estimation only when magnitudes of both VV and HH samples simultaneously exceed their thresholds. Even the first, arguably rather low threshold results in significantly different PDF (dashed line). The distribution narrows and shifts to lower values, although it still peaks close to the Bragg phase. The higher threshold causes the curve to further move towards smaller phase angles while its width does not seem to be much affected. This trend continues if the threshold level is increased.

Multilook averaging is another approach commonly used to stabilize and improve a phase estimate [1]. It involves adding up a number of independent samples (called “looks”) of complex channel products and evaluating the phase of the resulting sum (compare to (4)):

$$\varphi = \arg \left\{ \sum_{k=1}^N S_{HHk} S_{VVk}^* \right\} \quad (5)$$

In practice, such a summation can be accomplished by smoothing the data with a sliding window; the effective number of looks  $N$  is estimated as the ratio of the window size to the system resolution. This approach is adopted here with the Hann window applied in range direction. The 7.2-m effective width is estimated to result in a 25-look averaging. The PDF of the multi-look phase is plotted in Fig. 5. A single-look PDF from Fig. 4 (no threshold) is also shown. The behavior of the multi-look curve is similar to what was observed when a threshold was applied: the PDF narrows and shifts towards smaller phase values. Again, it is interesting to compare the simulated clutter distribution to the analytical result for the multi-look phase PDF based on the Gaussian assumption [1]:

$$p_\varphi^{(N)}(\varphi) = \frac{\Gamma(N+1/2)(1-\rho^2)^N \beta}{2\sqrt{\pi}\Gamma(N)(1-\beta^2)^{N+1/2}} + \frac{(1-\rho^2)^N}{2\pi} {}_2F_1(N, 1; 1/2; \beta^2) \quad (6)$$

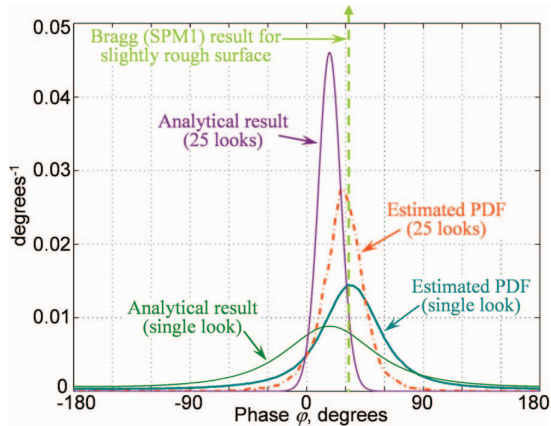


Figure 5. Probability density functions of phase difference between HH and VV backscatter evaluated from the simulated data upon multi-look averaging. Analytical predictions from (2) and (6) are also shown.

In (6),  ${}_2F_1$  is the Gauss hypergeometric function and  $\Gamma$  is the Gamma function. The values of  $\rho$  and  $\psi$  are those estimated earlier when evaluating (2) (the latter is a special case of (6) when  $N = 1$  [1] and is also plotted in Fig. 5 for reference). One observes an interesting pattern: while a single-look phase PDF of the simulated clutter is more compact than its analytical Gaussian-based counterpart, multi-look averaging does not cause the simulated PDF to narrow as much as would be expected for the underlying normal statistics. Also, the PDF for the multi-look phase difference of the simulated clutter still peaks well away from the average value of  $\psi = 17.6^\circ$ . These effects are probably due to the fact that the LGA sea backscatter is correlated with the long-scale wave field (e.g. [2], [5]), and the window size is still much smaller than the 23 m-long dominant wave on the surface.

#### IV. CONCLUSION

The non-Gaussian nature of the LGA sea clutter is manifested not only in its magnitude distributions, but has

apparent impact on phase between differently polarized echoes. Knowledge of such phase-difference statistics (or, preferably, joint amplitude-phase statistics for the polarization channels) is important for assessing the promise of sea-based polarimetric radar applications and is crucial for developing detection and parameter retrieval algorithms that rely on coherent polarization information. Polarimetric analysis may also prove to be another useful dimension for gaining insight into the mechanisms of the LGA sea backscatter.

#### REFERENCES

- [1] J.-S. Lee and E. Pottier, *Polarimetric Radar Imaging: from Basics to Applications*, CRC Press, Boca Raton, FL, 2009.
- [2] K. D. Ward, R. J. A. Tough, and S. Watts, *Sea Clutter: Scattering, the K Distribution and Radar Performance*. London, U.K.: Inst. Eng. Technol., 2006.
- [3] P. A. Hwang, B. Zhang, J. V. Toporkov, and W. Perrie, "Comparison of composite Bragg theory and quad-polarization radar backscatter from RADARSAT-2: With applications to wave breaking and high wind retrieval," *J. Geophys. Res.*, vol. 115, C08019, doi:10.1029/2009JC005995, 2010.
- [4] D. J. McLaughlin, N. Allan, E. M. Twarog, and D. B. Trizna, "High resolution polarimetric radar scattering measurements of low grazing angle sea clutter," *IEEE J. Ocean. Eng.*, vol. 20, no. 3, pp.166-178. Jul. 1995.
- [5] J. V. Toporkov and M. A. Sletten, "Statistical properties of low-grazing range-resolved sea surface backscatter generated through two-dimensional direct numerical simulations," *IEEE Trans. Geosci. Remote Sensing*, vol.45, pp. 1181-1197, May 2007.
- [6] T. Elfouhaily, B. Chapron, K. Katsaros, and D. Vandemark, "A unified directional spectrum for long and short wind-driven waves," *J. Geophys. Res.*, vol. 102, no. C7, pp. 15 781-15 796, 1997.
- [7] D. B. Creamer, F. Henyey, R. Schult, and J. Wright, "Improved linear representation of ocean surface waves," *J. Fluid Mech.*, vol. 205, pp. 135-161, 1989.
- [8] H.-T. Chou and J. T. Johnson, "Formulation of Forward-Backward method using novel spectral acceleration for the modeling of scattering from impedance rough surfaces," *IEEE Trans. Geosci. Remote Sens.*, vol. 38, no. 1, pp. 605-607, Jan. 2000.
- [9] G. R. Valenzuela, "Theories for the interaction of electromagnetic and ocean waves - a review," *Bound.-Lay. Meteorol.*, vol. 13, no. 1, pp. 61-85, 1978.